Coupling of Titania Inverse Opals to Nanocrystalline Titania Layers in Dye-Sensitized Solar Cells†

Seung-Hyun Anna Lee,‡ Neal M. Abrams,‡,¶ Paul G. Hoertz,‡,△ Greg D. Barber,‡,§ Lara I. Halaoui,⊥ and Thomas E. Mallouk*,‡

Department of Chemistry and Materials Research Institute, The Pennsylvania State University, University Park, Pennsylvania 16802, and Department of Chemistry, American University of Beirut, Lebanon

Received: March 28, 2008; Revised Manuscript Received: September 3, 2008

We report a quantitative comparison of the photoaction spectra, short circuit current densities, and power conversion efficiencies of dye-sensitized solar cells (DSSCs) that contain bilayers of nanocrystalline TiO_2 (nc-TiO_2) and titania inverse opal photonic crystals (PCs). Cells were fabricated with PC/nc-TiO_2 and nc-TiO_2/PC bilayer films on glass/tin oxide anode of the cell, as well as in a split configuration in which the nc-TiO_2 and PC layers were deposited on the anode and cathode sides of the cell, respectively. Incident photon current efficiencies at single wavelengths and current−voltage curves in white light were obtained with both cathode and anode side illumination. The results obtained support a model proposed by Miguez and co-workers, in which coupling of the low refractive index PC layer to the higher index nc-TiO_2 layer creates a standing wave in the nc-TiO_2 layer, enhancing the response of the DSSC in the red region of the spectrum. This enhancement is very sensitive to the degree of physical contact between the two layers. A gap on the order of 200 nm thick, created by a polymer templating technique, is sufficient to decouple the two layers optically. The coupling of the nc-TiO_2 and PC layers across the gap could be improved slightly by treatment with $TiCl_4$ vapor. In the bilayer configuration, there is an enhancement in the IPCE across the visible spectrum, which is primarily caused by defect scattering in the PC layer. There is also an increase of 20−50 mV in the open circuit photovoltage of the cell. With anode side illumination, the addition of a PC layer to the nc-TiO_2 layer increased the efficiency of DSSCs from 6.5 to 8.3% at a constant N719 dye loading of 155−160 nmol/cm^2.

Introduction

Dye-sensitized solar cells (DSSCs) were first introduced by Gratzel and co-workers in the mid-1980s[1] and have since been studied extensively. DSSCs represent a promising alternative to photovoltaic cells because they can be fabricated using inexpensive materials and proceses. While energy conversion efficiencies as high as 10.6% have been reported,[2] more typical values are below 8%, and higher efficiencies (especially for large area cells) are needed for DSSCs to become practical. The poor photoresponse of DSSCs in the red and near-infrared is one of the most important factors contributing to their low efficiency, since over 60% of the AM 1.5 solar power spectrum comes from wavelengths beyond 600 nm.[3] The widely used $(Bu_4N^+)_2[Ru(dcbpyH)_2(NCS)_2]^{2-}$ (N719, dcbpy = 4,4′-dicarboxy-2,2-bipyridine) dye[4] absorbs light weakly in the 600−750 nm region. Chemically related black absorber dyes have more recently been developed to extend the action spectrum of the DSSC further into the red with concomitant gains in efficiency.[5]

A complementary approach, which in principle can be used to extend the photoresponse of any dye, is to modify the optics of the DSSC. In the DSSC, the optically transparent anode is coated with a film of 15−20 nm diameter nanocrystalline TiO_2 (nc-TiO_2) particles. The nc-TiO_2 layer scatters light only weakly. However, when larger particles of TiO_2 are added, they increase the effective path length of light in the film through scattering. In 1997, Usami proposed a bilayer in which an overlayer of larger TiO_2 particles confined light to a thin nc-TiO_2 film on the DSSC anode through multiple scattering and total internal reflection.[6] Ferber et al. simulated light scattering effects in DSSC using Mie theory and the radiative transfer equation.[7] Their simulations showed that a mixture of small (D = 20 nm) and large particles (D = 125∼150 nm) can enhance photon absorption in DSSC. However, the ratio of the small particles and the large particles must be optimized since too many large particles increase the back-scattering and diminish the enhanced absorption. Rothenberger et al. performed simulations for the optimal optical design of the DSSCs and experimentally demonstrated that films made of a mixture of 65% small and 35% large TiO_2 particles (total thickness = 10 μm) and a double layer film composed of a 5 μm nc-TiO_2 film and a 5 μm scattering layer both resulted in a 6% increase of absorbed photon flux, mainly in long wavelength region (560∼750 nm).[8] Several experimental studies have verified that the inclusion of such scattering centers or layers can increase the short circuit current density and power conversion efficiency of the DSSC.[9−14]

We have previously found that photonic crystal (PC) scattering layers are effective in enhancing the red response of the DSSC. In our initial studies, we fabricated titania inverse opals on the anode electrode of the cell and covered them with nc-TiO_2 films, which were sensitized with the N-719 dye.[15] This

† Part of the "Janos H. Fendler Memorial Issue".

* To whom correspondence should be addressed. E-mail: tom@chem.psu.edu.

‡ Department of Chemistry, The Pennsylvania State University.

§ Materials Research Institute, The Pennsylvania State University.

⊥ Department of Chemistry, American University of Beirut.

¶ Current address: Department of Chemistry, SUNY ESF, Syracuse, NY.

△ Current address: Department of Chemistry, University of North Carolina, Chapel Hill, NC.

10.1021/jp802692u CCC: $40.75
Published on Web 10/17/2008

arrangement allowed us to study the effect of light localization in the bilayer but required an unconventional illumination of the cell through the cathode and electrolyte, which significantly reduces the performance of the cell. We postulated that the enhancement of incident photon current efficiency (IPCE) in the long wavelength region was induced by a standing wave effect in the photonic crystal. This effect has since been investigated by Ozin and co-workers as a means of enhancing the light absorbing properties of TiO_2 inverse opal photocatalysts.[16−18] While this model correctly predicted changes in the absorption spectrum of dye molecules confined to a TiO_2 inverse opal, the photonic crystal/nc-TiO_2 bilayer structure is more complex. In the bilayer film, resonant modes lead to enhanced absorbance by dye molecules in the nc-TiO_2 layer. Mihi and Míguez modeled the propagation of light in such bilayers and were able to reproduce the enhancement effect we observed in the IPCE.[19] According to their model, most of the photon absorption enhancement arises from light absorption in the nc-TiO_2 layer,[20] where most of the dye is adsorbed, and this is consistent with our observations.[21] Mihi et al. later verified experimentally that dye-sensitized TiO_2 inverse opals had poorer light absorption properties than single-layer nc-TiO_2 electrodes, consistent with their model, and showed that multiple inverse opal layers on nc-TiO_2 could provide spectral enhancement at multiple wavelengths.[22]

Although there have been subsequent reports of using colloidal crystals in different geometries as scattering layers for DSSCs, in general the performance of these cells has been poor.[23,24] These studies have therefore failed to address the question of whether a photonic crystal scattering layer will substantially improve the light-harvesting ability of state-of-the art DSSCs. Such DSSCs are illuminated from the anode side, and they contain nc-TiO_2 layers of optimized thickness. One goal of this study was therefore to fabricate nc-TiO_2/PC bilayer structures that could be illuminated through the anode and to quantify the effect of the added PC layer in optimized nc-TiO_2 cells. A second goal was to test an interesting prediction made by Mihi and Miguez,[19] that the introduction of a gap between the PC and nc-TiO_2 layers should disrupt the optical coupling of the two layers, thereby diminishing the enhancement of the IPCE in the spectral region to the red of the PC stop band. Scheme 1 shows the schematic structure of a dye cell containing a single nc-TiO_2 layer on a glass/fluorine-doped tin oxide (FTO) anode and the bilayer arrangements investigated in this work. The bilayers in panels a−c involve fabricating the titania inverse opal directly on the transparent conductor/glass substrate and then depositing a nc-TiO_2 layer, either on top of the PC layer or on the opposite electrode. Arrangements panels b and c allow us to test predictions of the Mihi-Miguez model.[19] The structure in panel d is more difficult to make, because it entails the fabrication of a titania inverse opal on top of the nc-TiO_2 layer without filling the interstices in the latter. We describe a new method for realizing this structure and compare the performance of such cells, illuminated from the anode side, with nc-TiO_2 cells that contain equivalent amounts of dye.

SCHEME 1: Configurations of DSSCs Investigated in This Work[a]

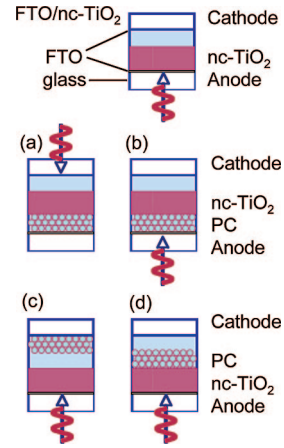

[a] Top: FTO/nc-TiO_2, illuminated from the anode side of the cell. (a,b) Previously studied configuration in which a titania inverse opal PC was fabricated on the anode and a nc-TiO_2 film was deposited on top of the PC layer. In panels a and b, this structure is illuminated from the cathode and anode sides, respectively. (c) Split configuration with the PC and nc-TiO_2 layers deposited on the anode and cathode with the cell illuminated from the cathode side. (d) Bilayer configuration in which nc-TiO_2 film was first deposited on the anode, and a PC layer was added by polymer templating. The thicknesses of the PC and nc-TiO_2 layers are typically 5−10 μm.

Experimental Section

Materials. Suspensions of monodisperse carboxylate-modified polystyrene spheres ($\langle d \rangle$ = 243, 291, 304, and 327 nm; 30, 10, 10, and 2 wt %, respectively, in water) were purchased from Seradyn, stored at 4 °C and used without further purification. Ammonium hexafluorotitanate ($(NH_4)_2TiF_6$, 99.99%, Aldrich), titanium isopropoxide (Aldrich), boric acid (H_3BO_3, 99.5% Alfar Aesar), *cis*-bis(isothiocyanato)bis(2,2′-bipyridyl-4,4′-dicarboxylato) ruthenium(II) bis(tetrabutyl ammonium) ($RuL_2(NCS)_2$-2TBA also known as Ruthenium535 bis-TBA, or N719, Solaronix), acetonitrile, and *tert*-butanol were used as purchased. The nc-TiO_2 particle slurry was synthesized according to published procedures but hydroxypropylcellulose [Aldrich, average M_W = 80 000] was used as a binder instead of Carbowax.[25] Titanium isopropoxide (35.52 g) and 10 mL of anhydrous isopropanol were added to a separatory funnel and mixed well. The Ti(i-OPr)$_4$/isopropanol solution was then added dropwise to 80 mL of acetic acid/250 mL of deionized H_2O in a round-bottom flask that had been prechilled to 0 °C in a dry ice/acetone bath. As the Ti(i-OPr)$_4$/isopropanol solution was added over a period of 20−30 min, the mixture was stirred rapidly with a magnetic stirring bar. The reaction solution was then heated to 80 °C and stirred rapidly for 8 h. After the solution was cooled down to the room temperature, it was sonicated using a cell disrupter for 5 min. The solution was then autoclaved at 230 °C for 12 h and then sonicated again for 5 min. The final concentration of TiO_2 was adjusted to 12 wt % with respect to total weight of solution. Hydroxypropylcellulose (HPC) was then added over 3−5 min to the rapidly stirred solution. The final HPC concentration was 6 wt % with respect to total weight of solution. The TiO_2 paste was first rapidly stirred for 24 h to dissolve HPC and the paste was continuously stirred less rapidly until its use. Electrodes were fluorine-doped tin oxide-coated glass substrates (FTO-glass, TEC8, Hartford Glass Co., IN, 8Ω/sq). All aqueous solutions were prepared with deionized water of resistivity ≥ 18.3 MΩcm.

Preparation of Bilayer Electrodes. FTO substrates (1 in. × 1 in.) were cleaned by sonication for 20 min in isopropanol and for 20 min in ethanol, followed by rinsing with deionized water and drying with air.

FTO/PC/nc-TiO_2 configuration (Scheme 1, panels a,b): Colloidal crystal films were grown following a modification of the method of Jiang et al.[26] Suspensions of carboxylate-modified polystyrene (PS) spheres in 60 mL of water were sonicated for

30 min to break up aggregates of particles. Before sonication, 0.3 g of a 0.5 wt % stock solution of nonionic surfactant, Igepal, was added to the PS suspension for better formation of a meniscus at the interface between the FTO and the solution. The FTO-glass substrates were immersed vertically in the PS suspension and the solvent was allowed to evaporate at 55 °C for 48 h. A 0.1 wt % PS suspension in water resulted in a 7−9 μm thick colloidal crystal film. Thinner films could be prepared by starting with lower PS concentrations in proportion to the desired thickness. The PS film was scraped off the back of the FTO-glass samples and kapton tape was applied to prevent TiO_2 deposition during the subsequent seeding and liquid phase deposition (LPD) steps. In the seeding step, the samples were immersed in a solution of 1.2% (weight/volume) of titanium isopropoxide and 0.12% HNO_3 in ethanol for 5 min at room temperature to grow a thin surface layer of titania on the polystyrene colloidal crystal. Following this step, the samples were held vertically and dried in air for several hours. In the subsequent LPD step, the samples were immersed vertically in an aqueous solution of 0.25 M boric acid and 0.20 M ammonium hexafluorotitanate for 30 min at 51 °C. The pH of the solution was first adjusted to 2.9 with 1 M HCl. After 30 min, the samples were rinsed thoroughly with deionized water and dried in air at room temperature. They were then calcined at 400 °C for 8 h to remove the PS spheres and create the inverse opal structure. The position of the stop band could be tuned by thickening the walls of the inverse opal in a second LPD step. The deposition time for this step, which typically shifted the stop band to the red by 10−20 nm, was approximately 30 min. Following this step, nc-TiO_2 paste was applied by the doctor-blade method. A few drops of nc-TiO_2 paste were deposited and spread onto the conductive side of the FTO/glass. Cellophane tape spacers with a thickness of 50 μm were applied to opposite edges of the electrode to control the thickness of the doctor-bladed nc-TiO_2 films. The samples were then calcined at 475 °C for 30 min.

FTO/nc-TiO_2 and FTO/nc-TiO_2/PC configurations (Scheme 1, panels c,d): To obtain the FTO/nc-TiO_2 structure for conventional DSSCs and the split bilayer structure shown in Scheme 1c, nc-TiO_2 paste was applied to the FTO-glass slide by the doctor blade method and cellophane tape was used to control the film thickness. The nc-TiO_2 films were heated in air at 5 °C/min to 405 °C for 30 min and then cooled to room temperature. For the FTO/nc-TiO_2/PC structure, two layers of a poly[(methyl methacrylate)-co-(methacrylic acid)] (80:20 and 75:25 = MMA/MA) copolymer, synthesized as described in the literature [T_g = 140 °C, average M_w = 129 000, average M_n = 58 000, M_w/M_n = 2.2],[27] were spin-coated onto the nc-TiO_2 film. The 5 wt % copolymer solution in *N*,*N*-dimethylformamide was dropped onto the substrate and spread evenly over the surface. After 1 min, excess solution was spun off the sample at 1600 rpm for 30 s. The substrates were heated at 150 °C for 30 s and allowed to cool before applying the second layer of copolymer. This copolymer layer prevents infiltration of the nc-TiO_2 film during the seeding and LPD steps. PS colloidal crystal layers were then grown, followed by TiO_2 seeding and a single LPD step as described above. The samples were then calcined in air at 400 °C for 8 h. During the calcination, the copolymer layer and the PS spheres are both burned away, leaving a TiO_2 inverse opal layer on top of nc-TiO_2 layer.

Electrode Assembly. Bilayer structures (FTO/nc-TiO_2/PC and FTO/PC/nc-TiO_2) were heated to 475 °C for 15 min, taken out of the furnace at 180 °C, then sensitized. The samples were slowly immersed into a 0.3 mM solution of N 719 dye in a mixture (50:50) of acetonitrile and *tert*-butanol to prevent cracking of TiO_2 and the substrate. All samples were sensitized for 48 h. The standard DSSC electrodes without PC layers underwent the same heating and sensitization steps.

After sensitization, the active area of the TiO_2 film was made to be 0.25 cm^2 by scraping away the excess. Stretched parafilm was used as a 20∼30 μm spacer between the anode and platinum counterelectrode. A drop of the redox electrolyte (see below)

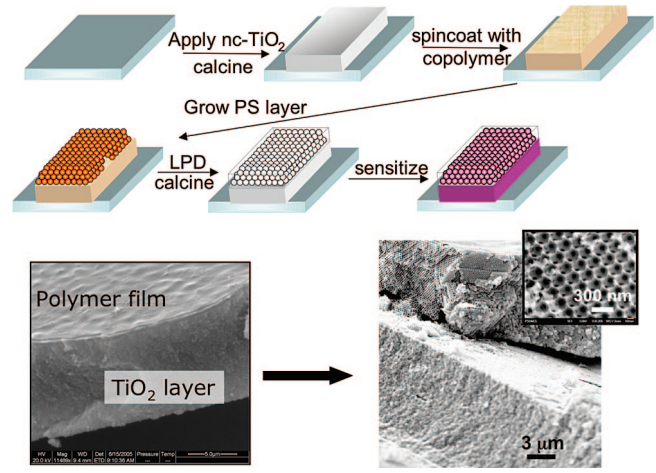

Figure 1. Schematic procedure for preparing FTO/nc-TiO_2/PC electrodes for the cell configuration shown in Scheme 1d. SEM images show the nc-TiO_2/polymer film before application of the PC layer, fabricated from 327 nm diameter PS spheres, and the final bilayer structure after the LPD and calcination steps. Inset shows a higher magnification image of the top of a TiO_2 inverse opal layer fabricated from 291 nm PS spheres.

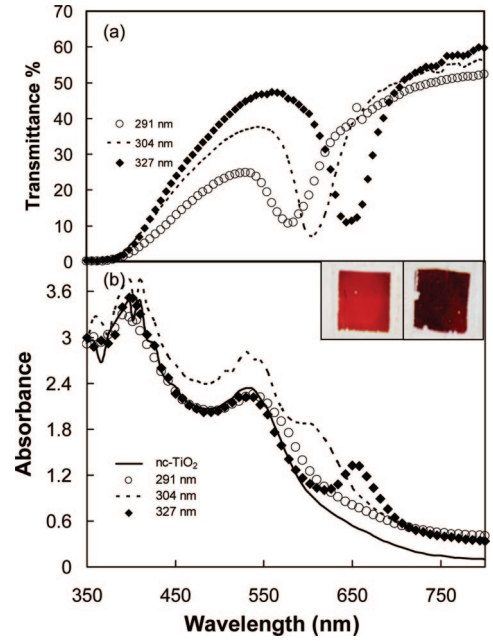

Figure 2. (a) Transmission spectra of unsensitized FTO/nc-TiO_2/PC bilayer structures made from 291 (open circles), 304 (dashed line), and 327 nm (crosses) PS spheres. Spectra were recorded in ethanol. (b) Normal incidence UV−vis absorption spectra (obtained in transmission mode) of a sensitized nc-TiO_2 film (solid line) and sensitized FTO/nc-TiO_2/PC bilayer structures made from 291 (open circles), 304 (dashed line), and 327 nm spheres (diamonds), recorded in acetonitrile. The background spectrum of an FTO-glass slide was subtracted to obtain the spectra shown. Inset shows sensitized FTO/nc-TiO_2 (left) and FTO/nc-TiO_2/PC bilayer (right) electrodes viewed from the back (i.e., the anode side).

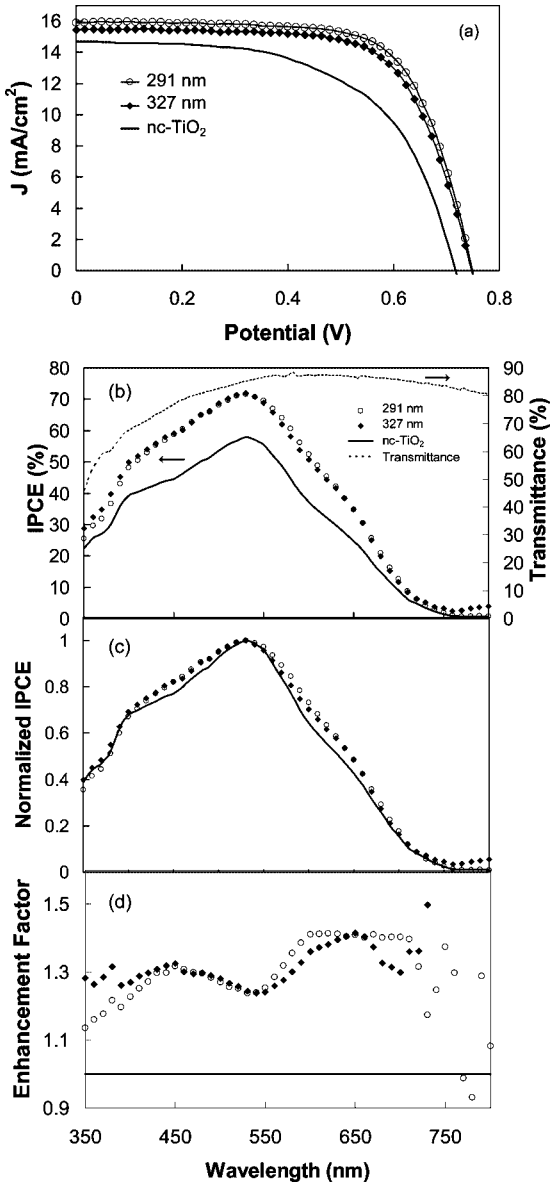

Figure 3. (a) Photocurrent vs photovoltage and (b) short circuit IPCE vs wavelength for FTO/nc-TiO_2 and FTO/nc-TiO_2/PC DSSCs with anode-side illumination (Scheme 1d): FTO/nc-TiO_2 (solid line), FTO/nc-TiO_2/PC (291 nm) (open circle), and FTO/nc-TiO_2/PC (327 nm) (diamonds). The dotted line in panel b represents the transmittance of the blank FTO-glass. IPCE was not corrected for reflectance or scattering losses of the FTO-glass. (c) IPCE spectra normalized to the maximum value, showing slight enhancement in both the blue and red spectral regions for the FTO/nc-TiO_2/PC cells, and (d) enhancement factor (the ratio of the IPCE to that of the FTO/nc-TiO_2 DSSC) vs wavelength. The bilayer resembles configuration d in Scheme 1.

was placed on top of the active area and a platinized FTO-glass counterelectrode was placed on it and secured using binder clips. For counterelectrode, a thin layer of Cr was first evaporated as an adhesion layer, then a 100 nm film of Pt was evaporated by e-beam onto 15-Ω FTO. A few drops of 5 mM hexachloroplatinic acid in anhydrous isopropanol were then deposited on the platinized electrode, which was dried and calcined at 385 °C for 15 min. For cells that were illuminated from the cathode side, the hexachloroplatinic acid solution was deposited on a bare FTO substrate and calcined at 385 °C for 15 min. The age of the Pt electrodes affects the fill factor of the cells significantly, so this step should be done shortly before assembly of the cell.

The redox couple/electrolyte solution consisted of 0.1 M LiI, 0.05 M I_2, 0.6 M 1,2-dimethyl-3-propyl-imidazolium iodide, 0.5 M tertbutylpyridine, and 0.1 M guanidinium isothiocyanate, which were dissolved in acetonitrile and sonicated for 30 min before use. 1,2-Dimethyl-3-propyl-imidazolium iodide was prepared according to the literature method.[28]

Photoelectrochemical Measurements. Electrical contact was made at the ends of the electrodes using alligator clips, and the cell was connected to a source meter (Keithley, Model 7002-HD). All current−voltage curves were obtained at 100 mW/cm^2 using AM 1.5 filters. A 150 W Xe Lamp (Oriel, Model 77250) was used as the light source. For incident photon current efficiency (IPCE) measurements, the short circuit current at each wavelength was obtained by passing light from the Xe lamp through a monochromator (Oriel 77250), which was scanned from 350 to 800 nm. A Si photodiode (Hamamatsu, S1226−44BK) was used to measure the spectral distribution of the incident power.

The amount of dye adsorbed onto the electrodes was determined spectrophotometrically (by UV−vis absorption) after desorption in 10 mL of 0.1 M NaOH in water/ethanol (50:50) solution for 5 h. Before the measurement, several drops of 0.2 M NH_4F(aq) were added to dissolve any TiO_2 residue from the film and thus eliminate the scattering background in the absorption spectra.

Analytical Instrumentation. UV−vis absorption and transmission spectra were collected using a diode array spectrophotometer (Hewlett-Packard, HP8452A). Scanning electron micrographs (SEM) were collected using a JEOL 6700F FESEM microscope operated at 5 kV, after sputtering a thin Ir film. A Tencor Instruments Alpha 3.7−2 profilometer was used to measure the thickness of the nc-TiO_2, copolymer, and bilayer films.

Results and Discussion

Fabrication of FTO/nc-TiO_2/PC Electrodes. In order to realize PC-coupled DSSCs that give red photocurrent enhancement without absorption losses in the blue, one must fabricate FTO/nc-TiO_2/PC bilayers that can be illuminated from the anode side. Unfortunately, any conformal deposition method that can convert the close-packed polystyrene sphere layer to a TiO_2 inverse opal can fill the mesoporous nc-TiO_2 layer as well. This can be prevented by first covering the nc-TiO_2 layer with a thin polymer film, as illustrated in Figure 1. In this figure, a ∼200 nm thick layer (as measured by profilometry) of 80:20 or 75:25 MMA/MA copolymer caps the nc-TiO_2 layer and prevents it from being infiltrated during the LPD process. The composition of the capping polymer is important in the deposition and LPD filling of the PS film. The water contact angle of the 80:20 copolymer surface was approximately 53°. If the copolymer is too hydrophilic, it is unable to protect the nc-TiO_2 layer during the LPD step. When a more hydrophilic commercial copolymer (40:60 = MMA/MA, Fluka) was used, the aqueous borate/hexafluorotitanate solution penetrated the polymer layer, causing the nc-TiO_2 film to delaminate. Figure 1 also shows an FE-SEM image of the final bilayer structure. The thickness of the inverse opal TiO_2 layer was typically 5−7 μm; this thickness can be easily adjusted by changing the concentration of PS spheres used in the growth of the film.

Figure 2a shows transmission spectra of the unsensitized bilayer structures in ethanol (n = 1.36), which has a similar refractive index to the solvent (acetonitrile, n = 1.34) used in the electrolyte of the DSSCs. All three spectra show pronounced stop bands, although the bands are broad because of the

TABLE 1: Summary Data from FTO/nc-TiO_2 and FTO/nc-TiO_2/PC DSSCs with Anode-Side Illumination[a]

	N719 surface coverage (nmol/cm^2)	total film thickness (μm)	J_{sc} (mA/cm^2)	V_{oc} (V)	fill factor	η (%)
FTO/nc-TiO_2 (10)	$110.0 \pm 0.5(100 \pm 20)$	10.0 ± 0.4	13.8 ± 0.7	0.75 ± 0.2	0.57 ± 0.04	5.9 ± 0.2
FTO/nc-TiO_2 (9)	$154 \pm 2(200 \pm 30)$	13.8 ± 0.6	14.7 ± 0.1	0.72 ± 0.01	0.612 ± 0.001	6.5 ± 0.2
FTO/nc-TiO_2/PC291 (11)	$159 \pm 2(200 \pm 20)$	15 ± 1	15.9 ± 0.5	0.750 ± 0.004	0.693 ± 0.004	8.3 ± 0.2
FTO/nc-TiO_2/PC327 (6)	$155 \pm 2(200 \pm 20)$	17 ± 3	15 ± 1	0.748 ± 0.001	0.679 ± 0.006	7.9 ± 0.5

[a] Each entry represents the average of two cells. For each type of cell, a total 6∼11 cells were prepared. The total number of samples for each type of cell is shown in parentheses in the first column. Because of the large sample-to-sample variation in dye adsorption, representative cells containing similar dye coverages were chosen for this comparison.

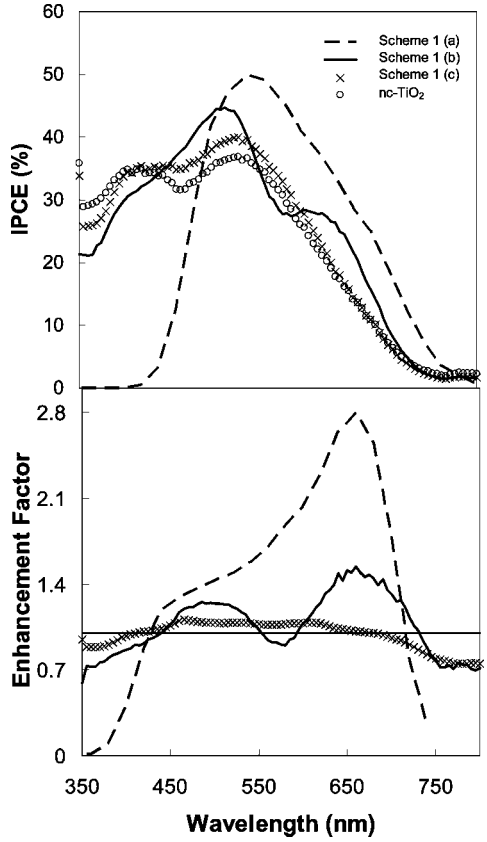

Figure 4. IPCE data (top) comparing a FTO/nc-TiO_2 DSSC with anode-side illumination (open circles) with the bilayer structures illustrated in Scheme 1a−c. Dashed line: FTO/PC/nc-TiO_2 cell with cathode side illumination (Scheme 1a). Solid line: Same cell, anode-side illumination (Scheme 1b). Crosses: Split bilayer cell, anode side illumination (Scheme 1c). The enhancement factor is shown at the bottom.

relatively small crystal domains in the PC structure. The small domain size, which is also evident in Figure 1, is most likely a consequence of the polydispersity of the PS spheres, which were 291 ± 1 nm, 304 ± 5, and 327 ± 5 nm, respectively. Because the lattice contracts approximately 30% during the PC fabrication and LPD processes, the diameters of the cavities formed from 291 and 327 nm PS spheres were 200∼210 and 230∼240 nm, respectively. These 291, 304, and 327 nm templates gave stop bands centered at 580, 605, and 650 nm, respectively which matched well to the calculated stop band maximum (λ_s) according to Bragg's law (1)

$$\lambda_s = 2d\sqrt{n_s^2 f + n_v^2(1-f)} \qquad (1)$$

where n_s is the refractive index of the surrounding medium (1.34), n_v is the refractive index of TiO_2 (2.54), the filling fraction (f) of TiO_2 is 26% for a closed-packed inverse opal structure, and d is the interlayer spacing, which is 0.87 times the diameter of the cavity. When these samples were sensitized with N719 dye, the absorption spectra shown in Figure 2b were obtained. As we previously observed with FTO/PC/nc-TiO_2 films, there is an enhancement in the apparent absorbance at the red edge of the stop band, resulting in a peak that shifts progressively to longer wavelengths with larger size PS template spheres.[15,21] This enhancement is visibly apparent in the reddish and dark brown to black appearance of sensitized FTO/nc-TiO_2 and FTO/nc-TiO_2/PC bilayer films, respectively. A strong scattering background is evident in all the spectra as a decreasing transmittance in the blue. Because this background is present in the FTO/nc-TiO_2 sample, it must arise primarily from the nc-TiO_2 layer. The bilayer structures have an additional diffuse scattering background in the red that apparently originates from the inverse opal layer.

DSSCs fabricated from FTO/nc-TiO_2/PC bilayer anodes showed consistently higher short-circuit current densities (J_{sc}) than did FTO/nc-TiO_2 DSSCs without scattering layers (Figure 3 and Table 1). An increase in open circuit photovoltage (V_{oc}) of 20−30 mV was also consistently found with the bilayer electrodes. Fill factor and power conversion efficiency comparisons tended to be more variable, because they were more dependent on the quality of the counter-electrodes used.

In reporting these data, typical cells were selected that contained approximately equal amounts of adsorbed dye. The thickness of the nc-TiO_2 film was optimized at 14−16 μm for FTO/nc-TiO_2 DSSCs. Thinner films gave lower dye coverages and lower J_{sc} values. For example, a 10 μm nc-TiO_2 film absorbed about 70% as much dye as did a 14 μm film, and consequently had lower J_{sc} (Table 1). Because the inverse opal layer was 5−7 μm thick, the nc-TiO_2 layer in the bilayer films was 9−11 μm thick. The bilayer cells and the thinner FTO/nc-TiO_2 cell have higher V_{oc} than the thicker FTO/nc-TiO_2 cell because there is less recombination between electrons in the TiO_2 and I_3^- ions in the electrolyte, as a consequence of the shorter average diffusion distance to the FTO surface. Decreasing the recombination rate results in a higher open circuit voltage.[29]

Figure 3 and Table 1 show that the short circuit current density (J_{sc}) increased by approximately 16 and 22% with 291 and 327 nm PC layers, respectively, relative to the 14 μm thick FTO/nc-TiO_2 DSSC. Surprisingly, this enhancement does not come from the increased red absorbance (Figure 2) of the bilayer electrode, because the shapes of the IPCE curves (Figure 3b) are very similar. By normalizing all the IPCE curves to their maximum value and by calculating the enhancement factor (Figure 3c,d), one can see that the increase in photocurrent comes from both the blue and red regions of the spectrum, implying that scattering enhances light absorption in the nc-TiO_2 layer across the spectrum.

TABLE 2: Summary data from FTO/nc-TiO_2 and FTO/nc-TiO_2/PC DSSCs that were treated with $TiCl_4$ prior to sensitization[a]

	N719 surface coverage (nmol/cm^2)	film thickness (μm)	J_{sc} (mA/cm^2)	V_{oc} (V)	fill factor	η (%)
FTO/nc-TiO_2	195 ± 7	15.6 ± 0.3	14.2 ± 0.2	0.721 ± 0.007	0.66 ± 0.03	6.7 ± 0.4
FTO/nc-TiO_2/PC (304 nm)	210 ± 8	18 ± 4	14.6 ± 0.3	0.747 ± 0.004	0.684 ± 0.004	7.4 ± 0.2
FTO/nc-TiO_2/PC (327 nm)	210 ± 7	19.1 ± 0.3	14.8 ± 0.1	0.740 ± 0.002	0.66 ± 0.04	7.2 ± 0.5

[a] Three samples of FTO/nc-TiO_2/PC304 (200 ± 20 nmol/cm^2) and PC327 (200 ± 10 nmol/cm^2) and ten samples of FTO/nc-TiO_2 (200 ± 20 nmol/cm^2) were prepared. Because of the sample-to-sample variation in the amount of dye adsorbed, cells with similar amounts of dye were compared in each case. Each entry represents the average of two such cells.

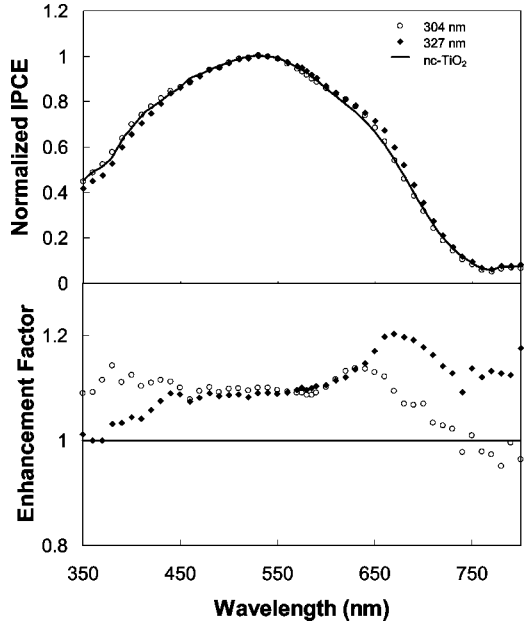

Figure 5. (a) IPCE spectra normalized to the maximum value for FTO/nc-TiO_2 and FTO/nc-TiO_2/PC DSSCs (Scheme 1d) with anode-side illumination, where the anode films were treated with $TiCl_4$ prior to sensitization: FTO/nc-TiO_2 (solid line), FTO/nc-TiO_2/PC (304 nm) (open circles), and FTO/nc-TiO_2/PC (327 nm) (diamonds). (b) The enhancement factor is the ratio of IPCE to that of the single-layer nc-TiO_2 DSSC. The bilayers are in configuration d from Scheme 1.

Three effects may contribute to the increase in photocurrent. First, the PC layer can act as a dielectric mirror, reflecting light that is transmitted by the nc-TiO_2 layer. However, this effect should be most pronounced in the stop band region and cannot explain the increased IPCE in the blue. A more likely effect, especially in the blue spectral region, is multidirectional scattering from defects in the PC layer.[30,31] Although simple computational models often do not account for the presence of the defects, defects in PCs can cause broadband diffuse scattering.[32] Both grain boundaries and voids in the PC layer are effective scattering layers. Hore et al. found that incorporating spherical voids as scattering centers in nc-TiO_2 films improved the efficiency of DSSCs by ~24%.[11] From Rayleigh scattering theory,[33] the intensity of scattering is inversely proportional with the fourth power of the wavelength. Hence, photons in short wavelength region should be more efficiently backscattered to the nc-TiO_2 film by defects in the PC layer. The weak enhancement to the red of the stop band is most likely caused by coherent scattering which gives rise to resonant modes in the nc-TiO_2 layer, as predicted in the Mihi−Miguez model.[19]

García-Santamaría et al. reported that the surface resonance mode created at the interface of PC layers and dielectric slab can be tuned and even removed by altering the geometry of the bilayer.[34] In that study, a high dielectric slab grown on top of opal structures was etched away and its effect on the surface resonance was investigated. As the high dielectric slab was progressively removed, the surface resonant mode was attenuated and finally vanished. By analogy, one should expect that when the nc-TiO_2 and PC layers are separated from each other by a rough interface or a gap on the order of half the wavelength of light, as appears in Figure 1, there should be little optical coupling of the two layers. To demonstrate the importance of the close physical contact of the bilayer, cells with split bilayers were prepared.

Spectral Response of Bilayer and Split-Layer FTO/PC/nc-TiO_2 Cells. Figure 4 compares short-circuit IPCE data for a FTO/nc-TiO_2 DSSC with no scattering layer, and for photonic crystal bilayer cells in the configurations shown in Scheme 1a−c. For the configuration in Scheme 1a,b, PCs were directly grown on the bare FTO electrode and nc-TiO_2 paste was spread on top of PC layers. This procedure results in intimate contact between the two layers as demonstrated previously[15] For the PC cells, 243 nm polystyrene spheres were used, and two LPD steps gave a stop band maximum of approximately 585 nm in ethanol.[21] This stop band maximum is 35 nm to the red of the IPCE maximum of the FTO/PC/nc-TiO_2 cell. With cathode-side illumination of the bilayer cell (Scheme 1a), the photocurrent is markedly enhanced in the spectral region (600−750 nm) to the red of the stop band maximum, as we have reported previously.[15,21] However, the current is also attenuated in the blue spectral region because of strong light absorption by the I^-/I_3^- redox electrolyte. With anode side illumination (Scheme 1b), there is a similar red enhancement, but reflection of light from the photonic crystal layer creates a wide notch in the IPCE spectrum in the vicinity of the stop band, as predicted by Mihi and Miguez.[19] Interestingly, the IPCE curve of the split bilayer cell (Scheme 1c) closely resembles that of the FTO/nc-TiO_2 cell. Additionally, the IPCE of the split bilayer experiment is remeniscent of that of the bilayer configuration in Scheme 1d (Figure 1) in which the IPCE increases slightly and across the whole spectrum relative to a FTO/nc-TiO_2 DSSC.

The striking difference between the split-layer spectrum (configuration c from Scheme 1) and those of the coupled bilayer cells (configurations a and b from Scheme 1) confirms that in the latter case, IPCE enhancement in the red region is not the result of a simple dielectric mirror effect. Intimate physical contact of the two layers is needed for optical coupling of the two layers. Hence, in order for configuration Scheme 1d to have the kind of red spectral enhancement as the configurations shown in Scheme 1b,c, the connectivity between the inverse opal layer and the nc-TiO_2 film must be improved. In an attempt to improve the connectivity, the bilayer electrodes were treated with 40 mM $TiCl_4$ at 70 °C for 30 min and then calcined at 475 °C for 30 min before sensitization. $TiCl_4$ treatment is often used in DSSC fabrication to increase the photocurrent, probably by improving the connectivity of the particle film, and more detailed experimental procedures are described in the literatures.[35] Table 2 summarizes the effect of this treatment with FTO/nc-TiO_2 and bilayer DSSCs. The bilayer structures have a higher loading of dye molecules than the FTO/nc-TiO_2 DSSCs. However, with such thick films, dye molecules anchored at the

most outer surface of PC layer do not contribute much to J_{sc} because of the inner filter effect of dye molecules closer to the FTO anode.[36] We again find an increase in the photocurrent and open circuit voltage with the addition of the scattering layer. The increase in photocurrent and power conversion efficiency is not as pronounced as it is without $TiCl_4$, possibly because of overfilling of the nano-TiO_2 film. Figure 5 shows that bilayers treated with $TiCl_4$ have a slightly increased red response, consistent with increased connectivity of the layers. However, the effect still appears very small compared with the dramatic increase seen in the intimately coupled FTO/PC/nc-TiO_2 bilayer (Figure 1).

Conclusions

The most important conclusion one can draw from this study is that intimate physical contact between nc-TiO_2 and TiO_2 inverse opal layers is needed to achieve strong red enhancement in the action spectrum of bilayer DSSCs. This effect is evident when one compares the IPCE spectra of the FTO/PC/nc-TiO_2 and split-layer cells (Figure 1). Those experiments are consistent with predictions of the Mihi-Miguez model.[19]

The new polymer templating method we describe allows one to fabricate FTO/nc-TiO_2/PC bilayer cells that can be illuminated from the anode side. In this case, a substantial increase in efficiency results from adding the scattering layer. The improvement in efficiency arises from an increase in both the photovoltage and the photocurrent at constant dye loading. Unfortunately, the method appears to result in a rough interface at the bilayer interface, and consequently we do not find a strong red enhancement in the IPCE of these cells. It is interesting that a dielectric band effect is apparent in the absorption spectra of dyes in these bilayers (Figure 2), but not in the IPCE spectra (Figure 5). This implies that the change in the absorption spectrum comes from light localization in the inverse opal layer, but because of poor coupling of the layers, this absorbed light does not contribute to the photocurrent. It will be interesting to explore other methods of fabricating this bilayer structure, for example, decal transfer methods, that can give better physical contact between the two layers.

In the poorly coupled FTO/nc-TiO_2/PC bilayers that we have fabricated, defect scattering appears to play a role in the enhancement of the photocurrent. We have previously found that disordered inverse opal layers in FTO//PC/nc-TiO_2 cells are also effective in enhancing the IPCE.[21] The roles of defects and disorder are still poorly understood and will be investigated in future work.

Acknowledgment. This work was supported by the U.S. Department of Energy, Office of Basic Energy Sciences, under contract DE-FG02-05ER15756.

References and Notes

(1) Desilvestro, J.; Grätzel, M.; Kavan, L.; Moser, J. *J. Am. Chem. Soc.* **1985**, *107*, 2988.
(2) Grätzel, M. *J. Photochem. Photobiol. B.* **2004**, *164*, 3.
(3) *American Society for Testing of Materials (ASTM) G173−03e1 Standard Tables for Reference Solar Spectral Irradiances: Direct Normal and Hemispherical on 37° Tilted Surface*; ASTM International: 2005.
(4) Nazeeruddin, Md. K.; Kay, A.; Rodicio, I.; Humphry-Baker, R.; Muller, E.; Liska, P.; Vlachopoulos, N.; Gratzel, M. *J. Am. Chem. Soc.* **1993**, *115*, 6382.
(5) Nazeeruddin, M. K.; Péchy, P.; Renouard, T.; Zakeeruddin, S. M.; Humphry-Baker, R.; Comte, P.; Liska, P.; Cevey, L.; Costa, E.; Shklover, V.; Spiccia, L.; Deacon, G. B.; Bignozzi, C. A.; Grätzel, M. *J. Am. Chem. Soc.* **2001**, *123*, 1613.
(6) Usami, A. *Chem. Phys. Lett.* **1997**, *277*, 105.
(7) Ferber, J.; Luther, J. *Sol. Energy Mater. Sol. Cells.* **1998**, *54*, 265.
(8) Rothenberger, G.; Comte, P.; Grätzel, M. *Sol. Energy Mater. Sol. Cells.* **1999**, *58*, 321.
(9) Vagas, W. E.; Niklasson, G. A. *Sol. Energy Mater. Sol. Cells.* **2001**, *69*, 147.
(10) Wang, Z.-S.; Kawauchi, H.; Kashima, T.; Arakawa, H. *Coord. Chem. Rev.* **2004**, *248*, 1381.
(11) Hore, S.; Nitz, P.; Vetter, C.; Prahl, C.; Niggemann, M.; Kern, R. *Chem. Commun.* **2005**, 2011.
(12) Hore, S.; Vetter, C.; Kern, R.; Smit, H.; Hinsch, A. *Sol. Energy Mater. Sol. Cells* **2006**, *90*, 1176.
(13) Koo, H.-J.; Park, J.; Yoo, B.; Yoo, K.; Kim, K.; Park, N.-G. *Inorg. Chim. Acta* **2008**, *361*, 677.
(14) Zhang, Z.; Ito, S.; O'Regan, B.; Kuang, D.; Zakeerudin, S. M.; Liska, P.; Charvet, R.; Comte, P.; Nazeerudin, M. K.; Péchy, P.; Humphry-Baker, R.; Koyanagi, T.; Mizuno, T.; Grätzel, M. *Z. Phys. Chem.* **2007**, *221*, 319.
(15) Nishimura, S.; Abrams, N.; Lewis, B. A.; Halaoui, L. I.; Mallouk, T. E.; Benkstein, K. D.; van de Lagemaat, J.; Frank, A. J. *J. Am. Chem. Soc.* **2003**, *125*, 6306.
(16) Chen, J. I. L.; von Freymann, G.; Choi, S. Y.; Kitaev, V.; Ozin, G. A. *Adv. Mater.* **2006**, *18*, 1915.
(17) Chen, J. I. L.; von Freymann, G.; Kitaev, V.; Ozin, G. A. *J. Am. Chem. Soc.* **2007**, *129*, 1196.
(18) Chen, J. I. L.; von Freymann, G.; Choi, S. Y.; Kitaev, V.; Ozin, G. A. *J. Mater. Chem.* **2008**, *18*, 369.
(19) Mihi, A.; Míguez, H. *J. Phys. Chem. B* **2005**, *109*, 15968.
(20) Mihi, A.; Míguez, H.; Rodríguez, I.; Rubio, S.; Meseguer, F. *Phys. Rev. B* **2005**, *71*, 125131.
(21) Halaoui, L. I.; Abrams, N. M.; Mallouk, T. E. *J. Phys. Chem. B* **2005**, *109*, 6334.
(22) Mihi, A.; Calvo, M. E.; Anta, J. A.; Miguez, H. *J. Phys. Chem. C* **2008**, *112*, 13.
(23) Ramiro-Manzano, F.; Atienzar, P.; Rodriguez, I.; Meseguer, F.; Hermienegildo, G.; Corma, A. *Chem. Comm.* **2007**, *3*, 242.
(24) Rodriguez, I.; Ramiro-Manzano, F.; Atinzar, P.; Martinez, J. M.; Meseguer, F.; Garcia, H.; Corma, A. *J. Mater. Chem.* **2007**, *17*, 3205.
(25) Zaban, A.; Ferrere, S.; Sprague, J.; Gregg, B. A. *J. Phys. Chem. B* **1997**, *101*, 55.
(26) Jaing, P.; Bertone, J. F.; Hwang, K. S.; Colvin, V. L. *Chem. Mater.* **1999**, *11*, 2132.
(27) Kiatkamjournwong, S.; Tessiri, S. *J. Appl. Polym. Sci.* **2002**, *86*, 1829.
(28) Bonhôte, P.; Dias, A.; Papageorgiou, N.; Kalyanasundaram, K.; Grätzel, M. *Inorg. Chem.* **1996**, *35*, 1168.
(29) Wang, Z.; Kawauchi, H.; Kashima, T.; Arakawa, H. *Coord. Chem. Rev.* **2004**, *248*, 1381.
(30) Koenderink, A. F.; Megens, M.; van Soest, G.; Vos, W. L.; Lagendijk, A. *Phys. Lett. A* **2000**, *268*, 104.
(31) Yip, C.-H.; Chang, Y.-M.; Wong, C.-C. *J. Phys. Chem. C* **2008**, *112*, 8735.
(32) Rengarajan, R.; Mittleman, D.; Rich, C.; Colvin, V. *Phys Rev. E* **2005**, *71*, 016615.
(33) Bohren, C. F.; Huffman, D. R. *Absorption and scattering of light by small particles*; John Wiley & Sons, Inc.: Weinheim, Germany, 1983.
(34) García-Santamaría, F.; Nelson, E. C.; Braun, P. V. *Phys. Rev. B* **2007**, *76*, 075132.
(35) (a) Wang, Q.; Ito, S.; Grätzel, M.; Fabregat-Santiago, F.; Mora-Seró, I.; Bisquert, J.; Bessho, T.; Imai, H. *J. Phys. Chem. B* **2006**, *110*, 25210. (b) O'Regan, B. C.; Durrant, J. R.; Sommeling, P. M.; Bakker, N. J. *J. Phys. Chem. C* **2007**, *111*, 14001.
(36) Ito, S.; Zakeerudin, S. M.; Humphry-Baker, R.; Liska, P.; Charvet, R.; Comte, P.; Nazeeruddin, M. K.; Péchy, P.; Takata, M.; Miura, H.; Uchida, S.; Grätzel, M. *Adv. Mater.* **2006**, *18*, 1202.

JP802692U